Three-dimensional physics studies in RFX-mod

L. Marrelli[1], E. Martines[1], A. Alfier[1], D. Bonfiglio[1], F. Bonomo[1], A.H. Boozer[2], A. Canton[1], S.Cappello[1], A.W. Cooper[3], D.F Escande[1], A. Fassina[1], P. Franz[1], M. Gobbin[1], S.P. Hirshman[5], P. Innocente[1], R. Lorenzini[1], P. Martin[1], B. Momo[1], N. Pomphrey[6], I. Predebon[1], M.E. Puiatti[1], D. Terranova[1], R. Sanchez[5], G. Spizzo[1], D.A. Spong[5], R.B. White[6], P. Zanca[1]

[1]Consorzio RFX, Associazione EURATOM-ENEA sulla Fusione, Padova, Italy
[2]Dept. of Applied Physics and Applied Mathematics, Columbia University, New York, NY
[3]EPFL, Association EURATOM-Confederation Suisse, Centre de Recherches en Physique des Plasmas, Lausanne, Switzerland
[4]Max Planck Institute für Plasmaphysik, Greifswald, Germany
[5]ORNL Fusion Energy Division, Oak Ridge, TN
[6]Princeton Plasma Physics Laboratory, Princeton, NJ

e-mail contact of main author: lionello.marrelli@igi.cnr.it

Abstract. In RFX-mod high current experiments the plasma frequently reaches the Single Helical Axis (SHAx) state, in which the core electron temperature assumes a helical shape and significant gradients appear. The plasma magnetic topology is strongly helical in the core while it is almost axisymmetric at the edge, thanks to the active control of the edge radial field. The weak helical field produced by the plasma profoundly affects the shape of the equilibrium going from 2D to 3D, therefore three-dimensional tools are being developed for the description of these states. On one hand the SHEq code, based on a perturbative approach, is used to determine the magnetic field topology. On the other hand, the VMEC code has been modified for the helical RFP, in order to describe the SHAx states by using tools developed by the Stellarator community. The effect of three-dimensional fields on transport is also being actively investigated. The magnetic shear is found to be correlated with regions with reduced transport: an investigation on the effect of 3D fields on transport mechanisms underlying such barriers is being performed by adopting several approaches.

1) Introduction

The discovery of Single Helical Axis States (SHAx) in the reversed field pinch (RFP) [1] gives a unique opportunity to investigate the physics of three-dimensional fields in magnetized fusion plasmas.

Thanks to its set of 192 independently controlled active coils [2,3], the RFX-mod experiment is well equipped to study these effects. In RFX-mod high current experiments, in fact, the plasma frequently reaches the Single Helical Axis (SHAx) state, in which the core electron temperature assumes a helical shape and significant T_e gradients appear. The SHAx states are the result of a spontaneous self-organization, which leads the current carrying plasma in a magnetic configuration with a strongly helical core (with *m=1*, n=-7 symmetry) embedded in an almost axisymmetric boundary. The weak helical field produced by the plasma profoundly affects the shape of the equilibrium going from 2D to 3D. This paper describes the advances in the description of such states: Sect. 2 recall the main assumption of the reconstruction algorithm of the helical equilibrium, based on a perturbative approach. In particular, it is shown that the q profile is flat in the core and differs from the axi-symmetric one. In Sect. 3 the results obtained of an alternative decription of the equilibrium, based on the VMEC code are described. While an overview on the progresses on the experimental characterization is given elsewhere [4,5], Sect. 4 recalls the effects of the helical geometry on transport as highlighted by means of a Monte Carlo approach and by considering the helical and toroidal ripple. In Sec. 5 a summary is presented.

2) Magnetic reconstruction of SHAx states: perturbative approach

Given the observation that the measured non-axisymmetric magnetic field amounts only to a few percent of the axisymmetric one, a first successful description of these states has been obtained by computing the perturbative solutions of the force balance equation in toroidal geometry with no pressure, performed by means of the NewCombToroidal code (NCT) [6].

The equilibrium magnetic field is considered as a superposition of an axi-symmetric part and a helical part due to the innermost resonant nonlinearly saturated resistive kink-tearing mode.

Axi-syimmetric equilibrium. The axi-symmetric part is obtained by solving the zero-th order force-free balance equation $J_0 \times B_0 = 0$, where the B_0 field is represented in straight field line coordinates (r, θ, ϕ)

$$B = \nabla F_0(r) \times \nabla \vartheta - \nabla \Psi_0(r) \times \nabla \phi$$

$F_0(r)$ and $\Psi_0(r)$ are the toroidal and poloidal fluxes respectively. Axi-symmetric flux surfaces are assumed to be non-concentric circles, each one labelled by its radius r, characterized by a horizontal shift $\Delta(r)$. It is assumed that $\sigma = J_0 \cdot B_0$ is constant along the surface, but can vary from surface to surface: While $\sigma(r)$ can be in principle any function, it is usually described by an analytical representation, depending on two free parameters $\sigma(r) = 2\theta_0/a\,(1 - (r/a)^{\alpha})$. The zero-th order force balance equation is then solved perturbatively and 5 ordinary differential equations are derived: 2 for the first order field components, 2 for the second order ones and one for $\Delta(r)$. Boundary conditions for this set of equations are edge measurements of $B_\theta(b)$ and of $\Delta(b)$, where b is the location of magnetic sensors. The $\sigma(r)$ profile, i.e. the α and θ_0 parameters, is then chosen in order to match $B_\phi(b)$ and the toroidal flux.

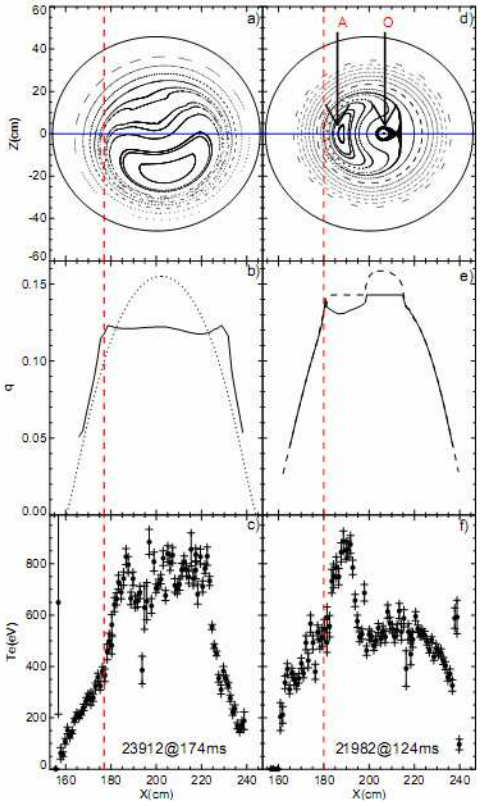

Figure 1) a),d) Poincaré pots for a SHAX and a DAx case. b) safety factor profile for a SHAx state (continuous) and q_{axi}. e) q for a DAx case. c),f) Thomson Scattering profiles along the diameters shown in a) and d)

Helical perturbations. Even when perturbations are present, the total field can be to cast in the form

$$B = \nabla F \times \nabla \vartheta - \nabla \Psi \times \nabla \phi$$

but F and Ψ are no longer constant on flux surfaces. The first order force-free balance equation, $j_1 \times B_0 + J_0 \times b_1 = 0$ is fourier decomposed and two linear ordinary differential equations (Newcomb equations) for the fourier coefficients of the F and Ψ functions are obtained

$$\Psi(r, \vartheta, \varphi) = \Psi_0(r) + \sum_{n \neq 0, m} \psi^{m,n}(r) e^{i(m\vartheta - n\varphi)} \qquad F(r, \vartheta, \varphi) = F_0(r) + \sum_{n \neq 0, m} f^{m,n}(r) e^{i(m\vartheta - n\varphi)}$$

Due to the toroidal geometry the equations for each n,m harmonic ($f^{m,n}$,$\psi^{m,n}$) are coupled to (n,m-1) ($f^{m-1,n}$,$\psi^{m-1,n}$) and to (n,m+1) ($f^{m+1,n}$,$\psi^{m+1,n}$). The details of the derivation of the equations as well as the solution technique are described in [6]. As far as the latter is concerned, the procedure is based on determining a base for the space of solutions to the equations for each n harmonic. The matching to experimental data is performed by computing, with the pseudo-inverse technique, the linear combination of the base solutions

that reproduces the Fourier component of each of the four arrays of radial and toroidal magnetic field measurements.

Magnetic field topology (DAx vs SHAx). These functions have been implemented in the ORBIT [7] and in the FLiT [8] field line tracing codes. Despite the fact that the helical field is rather small, the magnetic topology is significantly modified assuming a helical shape in the plasma core, which is correlated with the thermal content of the column.

Depending on the amplitude of the radial field, two kind of magnetic topology are found. If the field is below a certain threshold, the magnetic topology displays an island and the magnetic field is characterized by the presence of two magnetic axes (Double Axis, DAx) (Figure 1d). For such states a thermal helical structure winding around the magnetic axis is observed [9], characterized by an electron ITB [10] (Figure 1f). At higher values of the helical magnetic field, the field topology changes, as the axisymmetric O-point coalesces with the island X-point [11](Figure 1a). The former island O-point becomes the only magnetic axis, which motivates to term Single Helical Axis (SHAx) this kind of QSH state [12]. In SHAx states the region inside the ITB [13] spans a significantly bigger volume than in DAx states (Figure 1c).

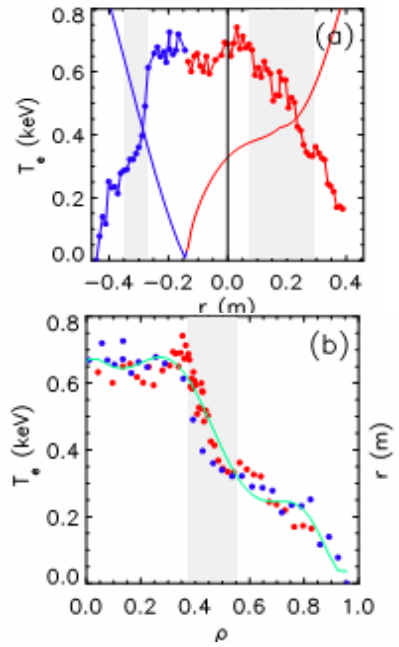

Figure 2) (a)Electron temperature measured along a horizontal diameter of RFX-mod (b) The same data of frame (a) plotted as a function of normalized the helical flux.

Computation of helical flux surfaces: The SHEq code. The electron temperature and density in SHAx states are constant on flux surfaces created by the *m=1,n=-7* perturbed field. The SHAx equilibria can be modelled as pure Single Helicity states, composed by the superposition of the zero-th order axisymmetric equilibrium and of the *m=1,n=-7* eigenfunction. The perturbed poloidal and toroidal fluxes are:

$$\Psi(r,u) = \Psi_0(r) + \psi^{1,7}(r)e^{iu} \qquad F(r,u) = F_0(r) + f^{1,7}(r)e^{iu}$$

where $u = \theta - 7\phi$ is an helical angle. It can shown that the function

$$\chi(r,u) = \Psi - 7F = \Psi_0 - 7F_0 + \psi^{1,7}(r) - 7f^{1,7}(r)e^{iu}$$

is constant on the helical flux surfaces, i.e. that $B\cdot\nabla\chi$ is constant over helical flux surfaces, and their shape can be determined without field line integration (as in [14]). This analytical representation allows re-mapping the profiles for diagnostics giving multi-point or multi-chord measurements, such as electron temperature by the TS diagnostics, electron density and SXR brightnesses.

The q profile of SHAx (and DAx) states and the electron transport barriers. The internal transport barriers observed in electron temperature profiles are associated with a flattening or a reversal of the magnetic shear profile of the helical QSH equilibria. This correlation is observed provided that the safety factor q of the helical surfaces is computed, which differs from the q profile of the axi-simmetric equilibrium (q_{axi}). The q value is computed using the helical flux function χ: if one adopts (χ,u,ϕ) as a new coordinate system, the magnetic field is represented by $B = \nabla F \times \nabla u - \nabla\chi \times \nabla\phi$. Considering the hamiltonian form of the magnetic field line equations, where ϕ is equivalent to time, u to coordinate, F to momentum and χ is the hamiltonian, a canonical trasformation to action-angle coordinates can be performed. This is achieved by computing the action as a loop integral over the constant-χ orbit

$$F_h = \frac{1}{2\pi}\int F(\chi,u')du'$$

The computation of the angle u_h conjugate to F_h is immaterial here: what matters is that in action-angle variable the trajectories (i.e. the magnetic field lines) are straight lines, and are characterized by a pitch equal to $\iota_h = d\chi\backslash dF_h$. Taking into account the 7-fold twist of the magnetic axis, one finally finds that $q=1/(\iota_h + 7)$. An example of the q profile for a SHAx states is shown in Figure 1b. For reference, the axisimmetric q_{axi} profile is also shown. While q_{axi} is greater than 1/7 in the core, the q value of all helical surfaces is always lower than 1/7: equivalently ι is always greater that 7. The q profile in SHAx states exhibits a maximum and its slope changes sign, implying the presence of a significant magnetic shear.

The concept of q is useful when analyzing DAx states too, (Figure 1d): the rotational transform is directly computed with a field line tracing technique, determining the total poloidal angle around the helical axis after one toroidal transit. For each surface, the definition is applied with respect to the axis it contains: q is less than 1/7 inside the magnetic island, while it is greater than 1/7, for the other surfaces. If the definition is applied considering an axis outside the surface, all the flux tubes are characterized by same value of q. Indeed the separatrix is the attractor of the X point, which is a remnant of the axi-symmetric resonant surface whose q_{axi} was exactly 1/7. The experimental relation between the positions of the electron temperature gradient foot and the shear reversal of q in both DAX and SHAx states, have been investigated statistically. A set of 55 reproducible shots have been considered. The location of the ITB has been determined by intersections of straight lines fitting the TS profiles in separate regions. In both the DAx and SHAx cases the two locations (Figure 3) are well correlated and coincide within a few cm. For the DAx case the steep gradient is systematically beginning slightly inside the separatrix, while for the SHAx case this gradient may be on any side of the maximum q surface. This may be due to the fact that in the SHAx case the separatrix expulsion reduces the level of the magnetic chaos. [11].

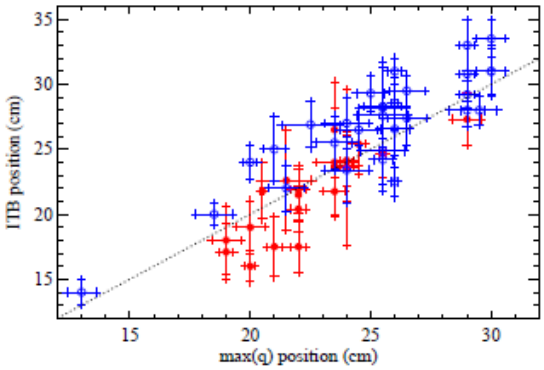

Figure 3) Position of the ITB vs the q maximum location for RFX-mod experimental DAx (full points) and SHAx states (empty points).

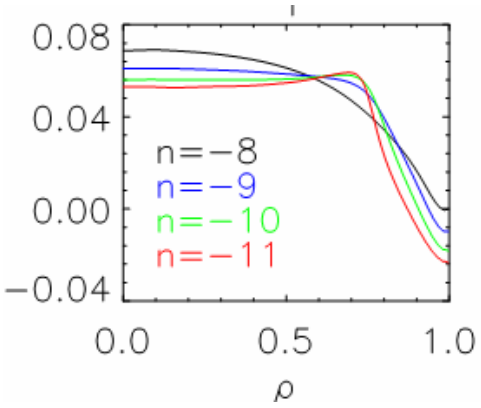

Figure 4) q profiles corresponding to different helical equilibria provided by visco-resistive MHD simulations (SpeCyl code) for m = 1 modes with n varying from n = −11 to n = −8.

The q profile in visco-resistive MHD simulations. The presence of a maximum in the q profile is also found in 3D MHD simulations performed in cylindrical geometry with the SpeCyl code [15], when the final SHAx state is the result of a transition from a DAx state. Helical equilibria are obtained in the code through the non linear saturation of a single perturbed m =1,n mode. The geometry of the SpeCyl simulations and their initial conditions are such that the inner most resonant mode is the n = −10. The q profile of the nonlinearly saturated helical state is obtained by applying the standard definition $d\psi_{tor}(\rho)/d\psi_{pol}(\rho)$. The shape of the q profile depends on the n number of the

mode (see Figure 4). In particular the n = −8 and n = −9 SHAx equilibria, which are obtained after the saturation of a non-resonant kink mode (without going through a DAxstate), are characterized by a monotonic *q* profile. On the other hand, when the SHAx equilibrium is reached as a saturation of a resonant resistive kink-tearing mode (as for −10 and for −11 helicities) i.e. after a transition from a DAx to a SHAx topology, the corresponding q profile takes a peaked shape.

3) Magnetic reconstruction of SHAx states: VMEC for the helical RFP

The helical states have also been described by the VMEC [16] code. Differently from tokamaks and stellarators, the RFP requires the poloidal flux as a surface label, due to the reversal of the edge toroidal field, and therefore the VMEC code has been modified [17,18]. At present, the code runs in fixed boundary mode and the toroidal periodicity number (N_{fp}) is set equal to 7, identical to the periodicity of the SHAx state. Differently from Stellarators and tokamaks this parameters is not set by the structure of the device but by the plasma. The shape of the surfaces is well represented by 9 poloidal harmonics and 6 toroidal harmonics. The experimental measurement of the toroidal flux at the LCMS is also set as a constraint.

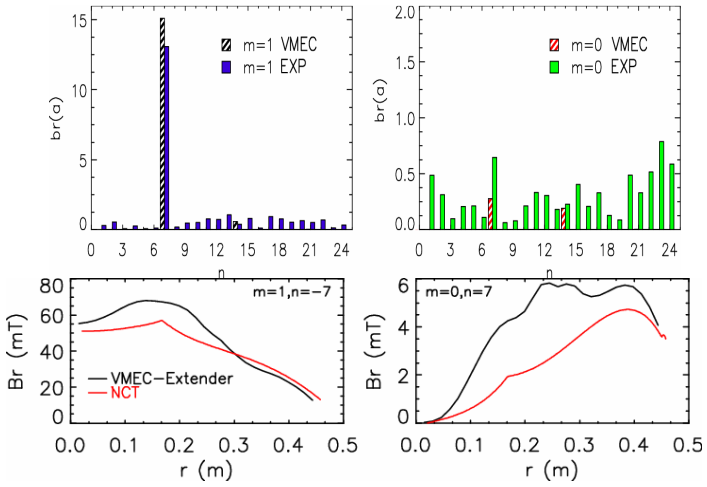

Figure 5) comparison between magnetic fluctuations spectra from experimental data and from VMEC:a) m=1 and b) m=0 radial field harmonic spectra ; c)m=1 and d) m=0 radial field inside the plasma

Differently from NCT, where the parallel axi-symmetric current profile $\sigma(r)$ needs to be defined, VMEC requires the $q(\rho)$ value for each flux surface. Finally, a guess for the displacement of the magnetic axis needs to be provided: this parameter is not a constraint but has an impact on the convergence. The code then computes the total plasma current, the shape of the surfaces and all the magnetic field and current density components along these surfaces. At present VMEC is not run to fit directly external measurements but uses the q profile computed by the SHEq code. Moreover NCT is used to define the shape of the LCMS, by computing the $\Delta_{1,7}$ and the $\Delta_{1,0}$ shifts ($\Delta_{0,7}$ shift are neglected in SHEq and therefore set to zero in VMEC). Given all of these inputs, VMEC computes the plasma current and the shapes of the helical magnetic surfaces which are in reasonable agreement with SHEq.

As a step towards a direct matching of the reconstructed equilibrium with the experimental measurements, the radial field due to the plasma currents only is computed by means of the EXTENDER code [19]. We neglect at present the fields produced by the currents flowing into the external conductors: the comparison of the radial harmonics (m=0 and m=1) is shown in Figure 5a,b. Given the choice of $N_{fp}=7$, only the 7, 14 and 21 harmonics can be compared to the experimental spectrum. The VMEC predicted amplitude is comparable to the experimental *m=1* harmonic. (Work is in progress in order to include the contribution of external currents, which requires taking into account the attenuation of the field due to the shell). We also compared the radial field inside the plasma: in this case the EXTENDER code computes the whole field, thanks to the virtual casing principle [19]. In order to ease the comparison, the VMEC fields are computed on a set of equally spaced points in the axi-

symmetric flux coordinates. In this way their Fourier transform is directly comparable to the eigenfunction profiles (see Figure 5c,d). The Newcomb approach for the first-order perturbation of the equilibrium in NCT assumes that a thin helical current density layer develops around the axi-symmetric resonant surface and a discontinuity in the first derivative of the radial field occurs. Such an assumption is not done in VMEC and the radial field derivative is not discontinuous.

Stability of helical equilibria. Though the helical states observed in RFX-mod last for several energy confinement times [20], temporary back transitions through reconnection events lead to a more chaotic, lower confinement state [21,22]. This at the moment prevents the helical equilibrium from being fully stationary. Numerically the stability of helical states has been addressed by means of MHD codes (3D but in cylindrical geometry) showing the importance of dissipation processes linked to both resistivity and viscosity, as well as the importance of the ratio between dominant and secondary modes [23,24] in non linear regimes.

As these analysis are quite demanding we attempted to address ideal linear stability of helical equilibria with the Terpsichore code [25], looking for periodicity breaking modes, i.e. modes that have a helicity close to the one corresponding to the dominant mode. Considering kink instabilities driven by parallel current, two examples have been considered with small differences in the safety factor profile: one case with a small reversed shear and one with a null shear in the helical core. As a preliminary result, it has been found that the helical states with monotonic q profile are significantly more unstable than the case with reversed shear, where the periodicity breaking modes are dominantly the $m=1,n=8$ coupled with the $m=2,n=15$ (both marginally resonant) components. As a direct extension of these results, a parametric study is presently underway to assess the role of the reversed shear region and of the resonances (also double resonances in the case of reversed magnetic shear) associated to the instability of periodicity breaking modes.

4) Effects of 3d geometry on transport in the helical RFP

Not only 3D fields significantly affect magnetic topology, but also play an important role in determining transport. Low confinement, globally axi-symmetric states, characterized by the simultaneous presence of many resonant modes, are in fact dominated by chaotic transport, but not far above the stochastic threshold. The resulting transport is subdiffusive, and cannot be described by Rechester-Rosenbluth diffusion [26]. It is found that whereas passing particles explore the stochastic field, the trapped particles experience normal neoclassical diffusion.

The presence of transport barriers in SHAx states near the location where the magnetic shear changes implies that magnetic chaos does not dominate transport.

Transport coefficients in helical states. Neoclassical effects and/or micro-turbulence might be ruling transport in the helical core and across the gradient of the internal barriers, even though the residual magnetic chaos could still play a role. An overview on the investigations on anomalous transport is presented elsewhere [5], we focus here on the effect of the helical geometry and of the residual magnetic chaos due to global tearing instabilities, whose eigenfunctions are well described by the NCT code.

Several approaches to study transport in helical states are being used: on the one hand volume averaged particle transport coefficients across helical surfaces are estimated numerically by a mono-energetic test particle approach [27]. This approach allows taking into account both the drifts of particles trajectories and the effect of the residual magnetic chaos. Work is in progress in order to implement in the ORBIT code also an electric field perpendicular to the helical surfaces. The numerical simulations only consider mono-energetic particles, subject to energy conserving collisions, in thermal equilibrium with the plasma background. Even though at higher electron temperatures (i.e. lower collisionalities) a global diffusion coefficient could not be defined, the average diffusion coefficient estimated with the

algorithm described in [27], do not significantly differ from the average of the local diffusion coefficients (estimated by computing $\Delta r^2/t$ with t chosen so that particles are still close to their initial deposition position, but large enough in order to observe the linear increase of Δr^2).

A complementary approach is based on the DKES code [28], which is based on VMEC equilibria, in order to estimate the full matrix of the local neoclassical transport coefficients, even though the effect of the residual magnetic chaos is not included. This approach is based on the assumption that transport can be described by a local approach: this assumption needs to be verified for RFX-mod experimental conditions.

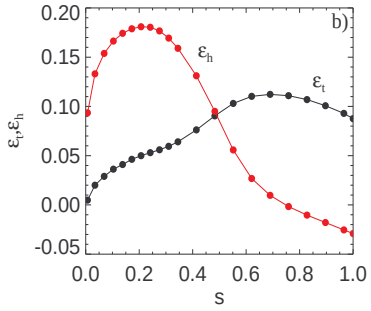

Figure 6) Radial profiles of the helical ε_h and of the toroidal ripple ε_t for a RFX-mod SHAx state.

As far as the Monte Carlo approach is concerned, in the ideal situation where no secondary modes are considered, at the density and temperature typical of RFX-mod, ORBIT gives $D_i \sim 0.8$ m²/s and $D_e \sim 0.06$ m^2/s, averaged over the whole helical domain. If residual chaos is taken into account D_i slightly increases to ~1 m^2/s, but a greater effect can be found on the electron diffusion (due to their small mass) and D_e can become of the order of 1-2 m^2/s. The different effect on the two species makes the implementation of a radial electric field necessary in order to ensure the ambipolarity constraint.

Helical magnetic ripple in SHAx states. The previous Monte Carlo results can be analyzed considering the magnetic field ripple profile, as it is usual in Stellarators [29].

The strong deviations from axi-symmetry of the core magnetic surfaces can, in fact, be quantified by means of the radial functions $\varepsilon_h(s)$ and $\varepsilon_t(s)$, the helical and the toroidal ripple respectively [29]. The radial dependences of these profiles are shown in Figure 6: ε_h is dominant in the central region ($\varepsilon_h \approx 2\text{-}3\ \varepsilon_t$) and close to zero at the edge ($\varepsilon_h \approx 0.1\text{-}0.2\ \varepsilon_t$). Thus, while the core is strongly helically deformed, the outer region almost preserves the typical properties of a quasi axisymmetric configuration. In regions where ε_h is high, particles with low parallel velocity may become helically trapped (superbananas), thus representing a significant source of losses due to their non-zero bounce averaged radial drift [29]. The trapped particle fraction in the helical state increases by about 10% compared to a standard axisymmetric RFP [30].

Neoclassical effects, and in particular super-bananas, which affects un-optimized Stellarators at low collisionality, might not be a significant issue for the helical RFP. The ORBIT code shows that when trapped particles drift out of the helical core, they reach a region ($r/a \sim 0.6$) where εh decreases and they become almost passing without being lost, at least at low collisionality. MonteCarlo transport simulations by ORBIT confirm that the ion diffusion coefficient (D_i) - volume-averaged over the helical domain - versus collisionality ν does not show the $1/\nu$ regime typical of Stellarators.

5) Summary

The SHAx states in the RFP share with the Stellarators the same helical nature, even though they rely on currents flowing into the plasma. The helical field produced by the plasma is relatively weak, and in fact it is relatively well represented by the perturbative approach. The basic ansatz behind this approach is the assumption that the axi-symmetric parallel current profile is a monotonically decreasing function of the radius with two parameters adjusted to match external magnetic measurements, and that the helical currents only flow in a thin layer around the resonant layer. On the other hand, the VMEC code computes the parallel current

(for the helical state) for a given q profile: at present, if the same q profile predicted by the perturbative approach is used, VMEC converge to an equilibrium which is similar to the perturbative one. Work is in progress in order to investigate if the q profile can be represented by few relevant parameters in order to infer its shape based on external measurements only. Work is also in progress in order to investigate the long term sustainment of the RFP reversal: an overview of recent progress on this subject is described elsewhere [5]. The vanishing of the magnetic shear is associated to an electron transport barrier: this indicates that magnetic chaos is no longer the dominant transport mechanism. Neoclassical effects on particle transport do not seem as critical in the helical RFP (characterized by rather high ι value) as in the Stellarator, due to the small drift of trapped particles (as computed by the ORBIT code) and the fact that helical core is actually surrounded by an axisymmetric configuration.

This contract was supported by the Euratom Communities under the contract of Association between Euratom/ENEA. The views and opinions expressed herein do not necessarily reflect those of the European Commission.

---

1 R. Lorenzini et al. Nature Physics 5 570-574 (2009)
2 P. Sonato, et al., Fus. Eng. Des. 66, 161 (2003)
3 T. Bolzonella, L. Marrelli, et al., EX/P5-01 this conference
4 M.E. Puiatti, M. Valisa, et al., EXC/P4-10 this conference
5 S. Cappello, et al., THC/P4-03 this conference
6 P. Zanca and D. Terranova, Plasma Phys. Controlled Fusion 46,1115 (2004).
7 I. Predebon, et al. Phys. Rev. Lett. 93, 145001 (2004)
8 P. Innocente et al., Nucl. Fusion 47, 1092 (2007)
9 P. Franz et al., Phys. Plasmas 13, 012510 (2006)
10 A. Alfier et al., Plasma Phys.Control.Fusion, 50, 035013 (2008)
11 D.F. Escande et al., Phys. Rev. Lett. 85, 3169 (2000)
12 R. Lorenzini et al., Phys. Rev. Lett. 101, 025005 (2008)
13 M. Valisa et al., Plasma Phys. Control. Fusion 50,124031 (2008)
14 M. Gobbin et al, Phys. Plas. 14, 072305-1, (2007)
15 S. Cappello, Plasma Phys. Contr. Fus. 46 B313 (2004)
16 S.P. Hirshman and J.C. Whitson, Phys. Fluids 26, 3554 (1983)
17 D. Terranova, M. Gobbin, et al., Contrib. Plas. Phys. 50, 775 (2010)
18 D. Terranova, et al, to be published, Plasma Phys. Contr. Fus. (52) (2010)
19 M. Drevlak, D. Monticello and A. Reimann, Nucl. Fusion 45, 731 (2005)
20 R. Lorenzini et al., Phys. Plasmas 16, 056109 (2009)
21 P. Piovesan et al., Nucl. Fusion 49, 085036 (2009)
22 M. Zuin et al., Plasma Phys. Control. Fusion 51, 035012 (2009)
23 S. Cappello,Theory of Fusion Plasmas, AIP Conference Proceedings, 27, 1069 (2008)
24 D. Bonfiglio et al., Nucl. Fusion 48, 115010 (2008)
25 W.A. Cooper et al., Fusion Sci. Technol. 50, 245 (2006)
26 G. Spizzo, et al., Plas. Phys. Contr. Fus. 51, 124026 (2009)
27 M. Gobbin, et al. Plas. Phys. Contr. Fus. 51 065010 (2009)
28 S.P. Hirsman et al., Phys. Fluids 29 (1986) 2951
29 H.E. Mynick, Phys. Plasmas 13, 058102 (2006)
30 M. Gobbin et al., J. Plasma Fusion Res. SERIES 8, 1147 (2009)